CORTEX 44 (2008) 936–952

available at www.sciencedirect.com

ScienceDirect

journal homepage: www.elsevier.com/locate/cortex

Special issue: Original article

Studying connections in the living human brain with diffusion MRI

*Derek K. Jones**

CUBRIC, Cardiff University Brain Research Imaging Centre, School of Psychology, Cardiff University, Cardiff, Wales, UK

ARTICLE INFO

Article history:
Received 7 June 2007
Reviewed 6 September 2007
Revised 24 October 2007
Accepted 9 December 2007
Published online 23 May 2008

Keywords:
Diffusion
MRI
White matter
Tractography
Connectivity

ABSTRACT

The purpose of this article is to explain how the random walks of water molecules undergoing diffusion in living tissue may be exploited to garner information on the white matter of the human brain and its connections. We discuss the concepts underlying diffusion-weighted (DW) imaging, and diffusion tensor imaging before exploring fibre tracking, or tractography, which aims to reconstruct the three-dimensional trajectories of white matter fibres non-invasively. The two main classes of algorithm – deterministic and probabilistic tracking – are compared and example results are presented. We then discuss methods to resolve the 'crossing fibre' issue which presents a problem when using the tensor model to characterize diffusion behaviour in complex tissue. Finally, we detail some of the issues that remain to be resolved before we can reliably characterize connections of the living human brain *in vivo*.

1. Introduction

In 1827, Robert Brown – a botanist from Montrose in Scotland, returned from a trip to Australia with various flora samples. Intrigued by the mechanisms of fertilization in plants, he took a sample of pollen grains from *Clarkia pulchella* and suspended them in water beneath his microscope (Fig. 1). On close inspection, Brown found the grains to be in constant motion – as if having a life of their own. Indeed, with investigations into the 'essence of life' being very much in vogue at the time, Brown wondered whether he was observing life force itself. However, as a true scientist, Brown looked for the phenomenon in inorganic material including rock and coal samples, and even '*rock from the Sphinx*'. He observed the same phenomenon, i.e., the particles were constantly in motion (Brown, 1828).

We now know that what Brown observed was not the pollen grains moving of their own accord, but rather the water molecules that they were suspended in (invisible under the light microscope) undergoing constant thermal agitation known as 'Brownian motion', or 'diffusion'. Diffusion is an essential physical process for the normal functioning of living systems. For example, the transport of metabolites into cells is facilitated by diffusion. This phenomenon, omnipresent in the water in living tissue, has the potential, through diffusion-weighted (DW) magnetic resonance imaging, to provide insights into cell physiology, cell structure and potentially the connections of the living human brain.

2. The random walk as a probe of tissue microstructure?

Imagine a cube-shaped volume of $2.5 \times 2.5 \times 2.5$ mm in dimension. There are approximately 10^{20} water molecules

* CUBRIC, School of Psychology, Cardiff University, Park Place, Cardiff CF10 3AT, UK.
E-mail address: jonesd27@cf.ac.uk
0010-9452/$ – see front matter © 2008 Published by Elsevier Masson Srl.
doi:10.1016/j.cortex.2008.05.002

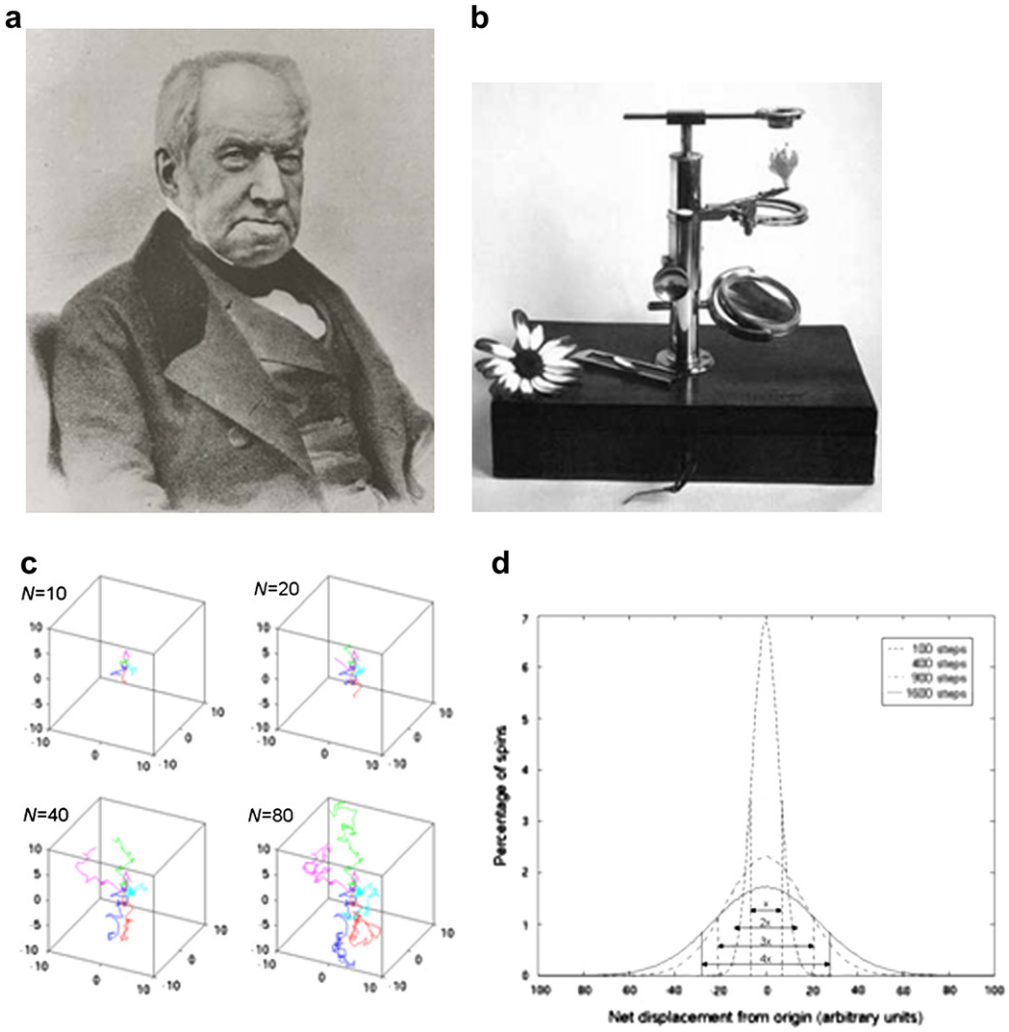

Fig. 1 – (a) Robert Brown, 1773–1858. (b) Brown's original microscope with which he reportedly observed the pollen of *Clarkia pulchella* in constant motion. (c) Simulation of trajectories of five molecules undergoing a random walk in an isotropic medium, after 10, 20, 40 and 80 steps. (d) A histogram of displacement from the origin of 1 million molecules, after 100, 400, 900 and 1600 steps. The full-width at half-maximum (FWHM) scales in the ratio of 1:2:3:4, which mirrors the ratio of √100√400:√900:√1600, demonstrating the consistency of Einstein's equation for Gaussian diffusion.

contained within this volume, each undergoing a random walk as part of the diffusion process. Here, by random walk, we mean that each molecule stays in a particular place for a fixed time, T, before moving to a random, new location in space. This process continues for each molecule so that a random path is drawn out in three-dimensional space. It would perhaps seem impossible to characterize the behaviour of this set of molecules undergoing such random behaviour. It is certainly impossible to predict the pathway that any one of these molecules will take. Fig. 1b shows a simulation of a random walk for five single particles in an isotropic medium, such as our cube of water. It is clear that we cannot accurately predict any single molecule's position at a given time. However, in 1905 Einstein proved that, provided the number of particles is sufficiently large, at least one aspect of the behaviour could be characterized, namely the squared displacement of molecules from their starting point over a time, t, averaged over all the molecules in the sample, $\langle r^2 \rangle$ is *directly proportional* to the observation time (Einstein, 1905). The constant of proportionality is the self-diffusion coefficient. In equation form (the "Einstein's equation"):

$$\langle r^2 \rangle = 6Dt \quad (1)$$

The distribution of squared displacements takes a Gaussian form, with the peak being at zero displacement and the probability of displacing a given distance from the origin is the same – no matter in which direction it is measured (Fig. 1d).

For the cube of water at body temperature (37 °C), the diffusion coefficient of water is $3 \times 10^{-3}\,\mathrm{mm^2\,s^{-1}}$. Thus, if we observe water molecules for, say, 30 ms, they will have displaced, on average, 25 μm in all directions.

As stated in Section 1, DW magnetic resonance imaging (MRI) utilizes this motion to probe tissue microstructure. The astute reader, new to the topic, may then pose the question "*If we are looking at the diffusion of water, and we know what the diffusion coefficient of water at body temperature is a*

constant – then how can we possibly use that to garner information about tissue microstructure?'' The answer lies in Einstein's equation (Eq. (1)), which says that the mean-squared displacement is directly proportional to the observation time. It is important to note that in DW MRI, we do not measure the diffusion coefficient directly, but the mean displacement of water molecules within each three-dimensional volume element, or voxel, that forms the image (typically, these are cube-shaped and about $2.5 \times 2.5 \times 2.5$ mm in dimension). The presence of cell membranes, inclusions, macromolecules and so forth present in tissue serve to hinder the pathway of the molecules undergoing their random walks. As a result, their overall displacement from their starting point in a fixed period of time is reduced and compared to their mean displacement when they were in 'free' water. Thus, it *appears* to us that the diffusion coefficient is lower than it is – which is partly why the term 'apparent diffusion coefficient' (or *ADC*) was coined to reflect the fact that we realize that we are subject to the effects of hindrances, etc. The average ADC in tissue is around 0.7×10^{-3} mm^2 s^{-1}, about 4 times smaller than in free water.

A DW magnetic resonance (MR) sequence sensitizes the MR signal to diffusion by imposing a given phase to a molecule that is dependent on its overall displacement (Stejskal and Tanner, 1965). Under the random walk process that is diffusion, we get a *distribution* of displacements and thus a distribution of phases. This spread of phases means a loss of signal coherence and therefore a reduction in signal amplitude, which in an image, means that the image appears darker. The greater the spread of displacements (the higher the ADC), the greater the spread of phases – and thus the greater the loss of signal – and the image appears dark. Conversely, the lower the rate of diffusion, the lower the spread of phases – and thus the lower the loss of signal and the image appears bright.

It is clear that tissue microstructure fundamentally affects the apparent diffusion properties of water and diffusion should therefore act as a sensitive probe to any changes in cellular structures that alter the displacement per unit time. Thus, the introduction of diffusion imaging (Le Bihan and Breton, 1985) was met with enthusiasm as a non-invasive method of gaining new contrast within the brain. The most useful clinical application to date is the use of the DW scan in acute ischaemia in which there is a reduction in the voxel-averaged displacement of water molecules per unit time, hence a reduction in the ADC, therefore less signal attenuation – and the lesion appears hyper-intense (Moseley et al., 1990a).

About the same time as Moseley's initial observations of the reduced ADC in ischaemia, it was noted that the ADC in certain regions of the mammalian brain appeared to depend on the direction of the applied diffusion-encoding gradient (Moseley et al., 1990b). In other words, the ADC was directionally dependent. This effect had been known for some time in ex vivo samples of muscle and brain tissue dating back to the pioneering work of Hansen (1971) and Cleveland et al. (1976). Shortly after Moseley's observation in the cat brain, the directional dependence of the ADC was reported in human white matter by Doran et al. (1990) and Chenevert et al. (1990). This is illustrated in Fig. 2, which shows the same (human) brain imaged 3 times, each time with the diffusion-encoding gradient applied along one of three orthogonal axes.

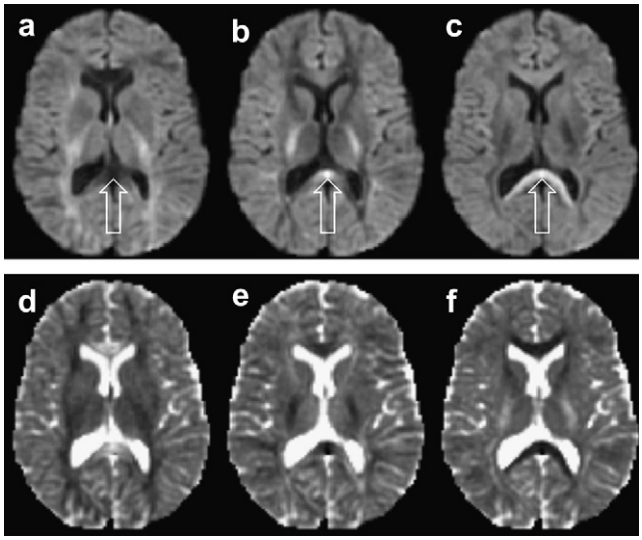

Fig. 2 – Effect of changing the direction of the diffusion-sensitizing gradients on the DW intensity (top row) and computed ADC (bottom row). The figure shows the same brain slice, with gradients applied in the left–right direction (a and d), anterior–posterior direction (b and e), and superior–inferior direction (c and f). The amount of diffusion weighting ($b = 1000$ s/mm^2) was the same in all three cases.

In certain regions of the brain, the DW intensity is the same in all three images suggesting that the ADC is the same in all directions. Diffusion in these cases is described as isotropic. However, in the regions highlighted by arrows this is not the case and diffusion in these regions is referred to as anisotropic. From just these three DW images, we can infer a substantial amount of information about the structure indicated by the arrows. First, the large differences in DW intensities that are observed as the direction of the diffusion-encoding gradient is changed, suggest that the tissue here is highly ordered on the voxel scale. Second, as there is high signal attenuation in 2a (in which the diffusion-encoding gradients were applied in a left–right orientation), we can infer that diffusion is relatively unhindered along this direction. Conversely, in the two perpendicular orientations (Fig. 2b and c), the signal attenuation is much less, indicating that the mean-squared displacement per unit time is reduced and that something is therefore hindering the displacement of water molecules along these orthogonal axes. Therefore, from just these three images, we are able to infer an ordered structure which has predominantly a left–right orientation. These inferences are entirely consistent with the fibres of the corpus callosum, a white matter (WM) structure which passes through this region (Dejerine, 1895; Crosby et al., 1962).

3. What is the source of diffusion anisotropy?

Initial suggestions for the mechanisms underlying diffusion anisotropy in WM included the myelin sheath (Thomsen

et al., 1987), local susceptibility gradients (Hong and Dixon, 1992; Lian et al., 1994), axonal cytoskeleton and fast-axonal transport. Myelin itself, however, does not appear to be necessary in order for diffusion to be anisotropic in the brain. This conclusion was first suggested by the demonstration of anisotropic diffusion in the immature rat brain where there was no histological evidence of myelin (Wimberger et al., 1995; Prayer et al., 1997). Furthermore, Gulani et al. (2001) reported anisotropic diffusion in the spinal cord of a myelin-deficient rat. In the mid-1990s, Christian Beaulieu and Peter Allen conducted a series of experiments to try to elucidate the origin of anisotropy in WM (Beaulieu and Allen, 1994a, 1994b, 1996) and were able to rule out the effects of susceptibility induced gradients, axonal cytoskeleton and fast-axonal transport. They concluded that the main determinant of anisotropy in nervous tissue is the presence of intact cell membranes and that myelination serves to modulate anisotropy. For a thorough and excellent review, see Beaulieu (2002).

4. The diffusion tensor

It should be clear that, in contrast to our cube of free water, when we have ordered tissue in our sample, we can no longer characterize the behaviour of the water molecules with a single ADC. The ADC we measure will depend on the direction in which we measure it. The more ordered the tissue is within the sample, the more the ADC will depend on the measurement direction. The next most complex model to characterize Gaussian diffusion in which the displacements per unit time are not the same in all directions is the diffusion tensor. This is a 3×3 symmetric matrix of numbers that characterizes three-dimensional displacements. The diagonal elements correspond to diffusivities along three orthogonal axes, while the off-diagonal elements correspond to the correlation between displacements along those orthogonal axes. For those less mathematically inclined, the tensor can be thought of in another way. Consider a gedanken experiment in which we place a drop of ink in the centre of our cube of water. As the ink particles displace over time, the outer profile of the displacements would resemble a spherical envelope, since diffusion in isotropic media is isotropic. However, in an anisotropic medium, the ink particles would diffuse further along the principal axis of the anisotropic medium than in a perpendicular orientation. Clearly, the displacement profile can no longer be described by a sphere and is more correctly described by an ellipsoidal envelope with the long axis parallel to the long axis of the anisotropic medium (Fig. 3). The diffusion tensor is often thought of in terms of this ellipsoid – a surface representing the distance that a molecule will diffuse to with equal probability from the origin. The diffusion tensor formalism provides an 'internal reference frame', namely the eigensystem. The principal axes of the ellipsoid are given by the eigenvectors, and the lengths are given by the diffusion distance in a given time, t. Eq. (1) shows that the displacement in a given time is proportional to the square root of the diffusivity. Hence, the ellipsoid axes are scaled according to the square root of the eigenvalues. The tensor is estimated by collecting a number of samples of the DW signal, the direction in which the diffusion sensitization is applied being varied for each sample. The tensor is subsequently estimated from these signals using multivariate regression. Full details are provided in Beaulieu and Allen (1994a).

5. Trace

The trace of the diffusion tensor is equal to the sum of its three eigenvalues and provides a rotationally invariant index of the overall amount of diffusivity within each image voxel. It is equivalent to 3 times the average diffusivity and so a more commonly reported index is the 'mean diffusivity' which is the trace divided by three. The trace can also be computed by taking the average of three ADCs measured along any three orthogonal axes.

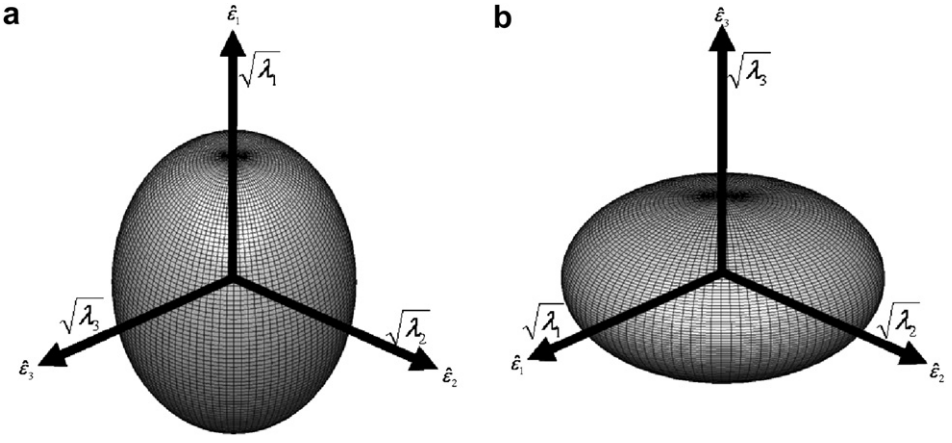

Fig. 3 – Schematic of the diffusion ellipsoid. The ellipsoid is the envelope where a spin – placed at its centre – will diffuse to with equal probability. The axes are scaled according to the square root of the eigenvalues, λ_1 λ_2, and λ_3, and the principal axes are given by the corresponding eigenvectors, ε_1, ε_2, and ε_3. The eigenvalues are sorted according to their magnitude such that $\lambda_1 \geq \lambda_2 \geq \lambda_3$. The tensor in (a) is prolate, where $\lambda_1 > \lambda_2 = \lambda_3$. The principal eigenvector is designated as ε_1. In (b), the tensor is oblate, i.e., $\lambda_1 = \lambda_2 > \lambda_3$ and the principal eigenvector is therefore poorly defined.

6. Diffusion anisotropy

The eigenvector/eigenvalue system provides a framework that rotates with the diffusion tensor, and thus any index of anisotropy that is defined within this framework, will be independent of the orientation of the tensor with respect to the laboratory frame of reference. By far, the two most commonly used indices are the relative anisotropy (RA) and fractional anisotropy (FA) (Basser and Pierpaoli, 1996).

$$RA = \sqrt{\frac{1}{3}}\frac{\sqrt{(\lambda_1-\bar{\lambda})^2+(\lambda_2-\bar{\lambda})^2+(\lambda_3-\bar{\lambda})^2}}{\bar{\lambda}} \quad (2)$$

$$FA = \sqrt{\frac{3}{2}}\frac{\sqrt{(\lambda_1-\bar{\lambda})^2+(\lambda_2-\bar{\lambda})^2+(\lambda_3-\bar{\lambda})^2}}{\sqrt{\lambda_1^2+\lambda_2^2+\lambda_3^2}} \quad (3)$$

where $\bar{\lambda} = (\lambda_1+\lambda_2+\lambda_3)/3$.

The numerator for both terms is the same and is related to the variance of the three eigenvalues about their mean. The FA index normalizes this measure by the magnitude of the tensor as a whole. Just as the magnitude of a vector can be found from the sum of the squares of its individual components, the magnitude of the tensor is found from the sum of the squares of its eigenvalues. Thus, FA measures the fraction of the tensor that can be assigned to anisotropic diffusion. The FA index is appropriately normalized so that it takes values from 0 (when diffusion is isotropic) to 1 (when diffusion is constrained along one axis only). The denominator of the RA index is simply the mean diffusivity. This index is mathematically identical to a coefficient of variation, i.e., standard deviation divided by the mean. Fig. 4 shows an example FA map in axial and coronal formats. The higher the pixel intensity, the higher the FA, thus gray matter and cerebro-spinal fluid (CSF) appear dark, while white matter appears, on the whole, bright. Voxels that contain fibres that run in highly parallel

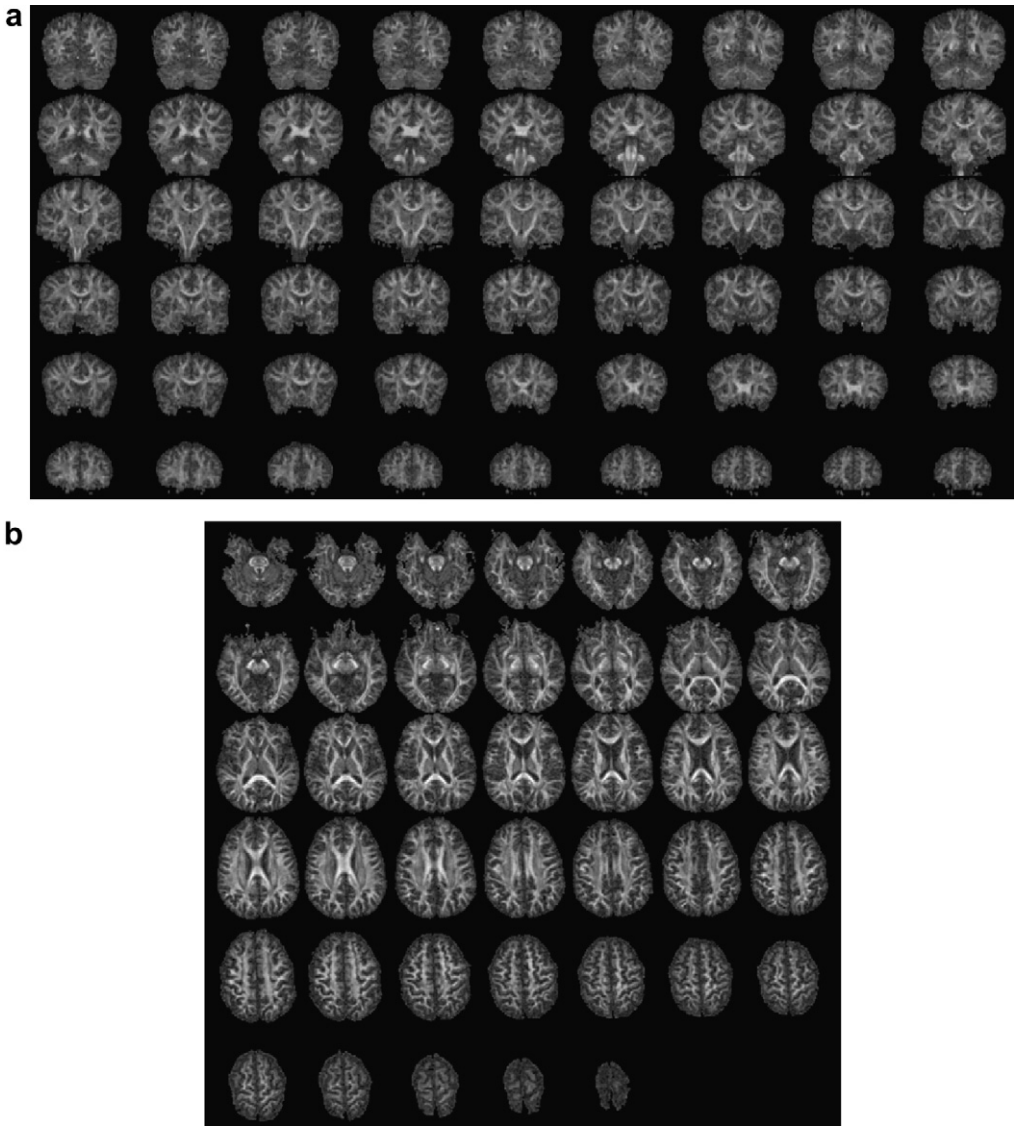

Fig. 4 – Example FA images from the whole brain in (a) coronal and (b) axial orientations. The pixel intensity is directly proportional to the FA which ranges from zero (diffusion is isotropic) to the theoretical limit of 1 (where water molecules are only free to move along one axis).

fashion (e.g., voxels in the corpus callosum and cerebral peduncles) appear the brightest.

7. Tensor orientation

We saw in Fig. 2 that for structures predominantly oriented along the principal axes (*x*, *y* and *z*), it was possible to infer fibre orientation from three DW images or three ADC images in which the diffusion encoding was applied along those three orthogonal axes. Early work attempted to capitalize on this ability and approaches were proposed for creating fibre orientation maps based on ADC measurements (Douek et al., 1991; Nakada et al., 1994). However, as should now be clear from previous discussion, these maps are rotationally variant. Jones et al. (1997) and Pierpaoli (1997) showed how robust and readily interpreted fibre orientation maps could be derived by using the information contained within the diffusion tensor (more specifically, the principal eigenvector, i.e., the eigenvector associated with the largest eigenvalue). The key idea is that components of the orientation of the fibre are represented using different primary colours. Fig. 5 shows an example of the 'absolute

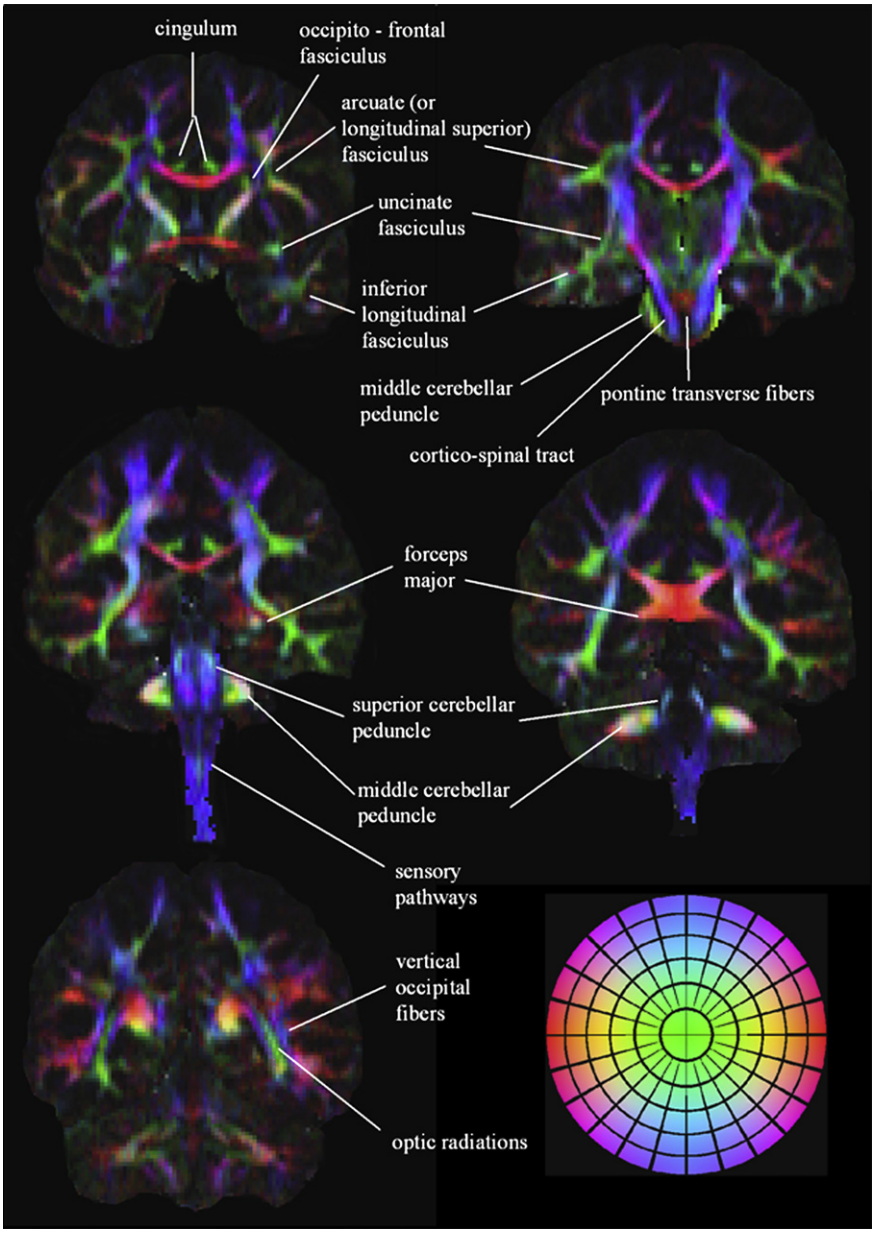

Fig. 5 – Example of colour encoded fibre orientation maps. Fibres that are predominantly oriented left–right are shown in red, anterior–posterior fibres are shown in green and superior–inferior fibres are shown in blue (see colour wheel at lower right hand corner). Comparing these images with those in Fig. 4(b), it is clear that the colour maps provide more information than anisotropy maps alone. Figure taken from Pajevic and Pierpaoli (1999). ©1999 Reprinted by permission of Wiley-Liss, Inc. a subsidiary of John Wiley & Sons, Inc. The author is grateful to Dr. Carlo Pierpaoli, National Institute of Child Health and Human Development, Bethesda, MD, for supplying the figure. [For interpretation of colour in this figure legend the reader is referred to the web version of the article.]

direction' scheme proposed by Pajevic and Pierpaoli (1999), the most commonly used scheme to date. Makris et al. (1997) used colour-coded fibre orientation images (derived from diffusion tensor MRI (DT-MRI) data), combined with *a priori* knowledge of the location and pathways of white matter fasciculi, to produce a series of two-dimensional coronal images within which the major fasciculi were identified. The individual fasciculi were clearly delineated due to abrupt changes in fibre orientation at the boundaries of fasciculi, and the authors demonstrated correlation between colour-coded fibre orientation images and an anatomical map of the human brain (Dejerine, 1895), highlighting the potential of using DT-MRI to study the morphometry of white matter fasciculi. However, visualization of the three-dimensional morphometry of a particular fasciculus in its entirety using data presented solely in a two-dimensional format is difficult.

8. Following pathways and their connections

On viewing fibre orientation in one voxel and following a path of smooth transition in colour from one voxel to the next, one can gain an impression of the trajectory of the major WM pathways. Originated in the late 1990s, the purpose of fibre tracking or 'tractography' is to infer the three-dimensional trajectories of anisotropic structures in tissue by piecing together discrete (voxel-based) estimates of the underlying *continuous* fibre orientation field (Conturo et al., 1999; Jones et al., 1999; Mori et al., 1999; Basser et al., 2000; Parker, 2000; Parker et al., 2003; Poupon et al., 2000; Tuch et al., 2000; Koch et al., 2001). Fibre tracking algorithms can be broadly classified into two types: deterministic and probabilistic.

Initial work in the field focused on the former, i.e., deterministic tractography (e.g., Conturo et al., 1999; Mori et al., 1999). The implicit underlying assumption is that the principal eigenvector, ε_1 (i.e., the eigenvector associated with the largest eigenvalue, λ_1) is parallel to the underlying dominant fibre orientation in each voxel (Basser et al., 1994) and forms a tangent to the space curve traced out by the white matter tract (Basser et al., 2000). The evolution of the space curve is therefore performed by propagating a *single* pathway bi-directionally from a "seedpoint" (usually the centre of an image voxel), by moving in a direction that is parallel with ε_1. Crucially, it is assumed that the underlying tensor field is continuous and therefore, as the step size is usually fixed (e.g., to a 10th of the voxel dimension), sub-voxel estimates of the tensor are required for this approach. These are obtained either by interpolation of the raw DW images prior to re-estimation of the tensor (Conturo et al., 1999), or by interpolation of the tensor elements – either by simple trilinear interpolation, or by fitting a continuous model of the underlying field using third order B-splines (Aldroubi and Basser, 1999; Pajevic et al., 2001). Essentially, this allows an estimate of the tensor field to be obtained at any arbitrary point within the imaged region, i.e., not just at the centre of an image voxel, by fitting a series of mathematical functions to the data.

An alternative approach to deterministic tractography was proposed by Mori et al. (1999) The FACT method (fibre assignment by continuous tracking) does not assume that the underlying fibre trajectory is continuous, but rather that the fibre orientation is uniform everywhere within a voxel, and changes abruptly at the boundary of a voxel. The step length is no longer constant since the path is propagated from the seedpoint, parallel to the principal eigenvector until the boundary of the voxel is encountered, at which point the algorithm traverses the next voxel in a direction parallel to the eigenvector at the centre of this new voxel.

There are two arbitrary thresholds often employed to constrain the tractography. The first is that tracking is terminated if the front of the tract enters a region where the anisotropy is below a fixed value (most often chosen to be the threshold that differentiates white matter from gray matter). The motivation for this threshold is to prevent the tract reconstruction from entering into the gray matter and/or regions where the principal fibre orientation is poorly defined. A second threshold often applied is an angular threshold, i.e., the maximum angle that the path can turn through between one step and the next. The aim is ultimately to prevent 'unfeasible' turns in fibre orientation and prevent, for example, the tract reconstruction from doubling back on itself. There is, however, no general consensus in the literature as to what this angular threshold should be and depends on the anatomy, step size and voxel dimensions.

In using deterministic tracking packages, the user invariably selects more than one seedpoint (voxel) from which to initiate tracking, and typically selects a region of interest (ROI) which, (and importantly), based on prior anatomical knowledge, intersects the fasciculus of interest. Fig. 6 gives a basic illustration of the principle of deterministic tract reconstruction from an ROI placed in the splenium of the corpus callosum. For tracts where it is possible to define such an ROI where the user can be absolutely certain that no other fasciculi are included, (e.g., in the splenium of the corpus callosum at the midline), this approach performs adequately. However, it is known from classical neuroanatomy studies (e.g., Dejerine, 1895; Ludwig and Klingler, 1956; Crosby et al., 1962) that cerebral white matter is mainly composed of different fasciculi that run closely to one another. Thus, for many fasciculi of interest, it is difficult to define a single ROI that includes only the fibres of the fasciculus of interest. A solution to this problem is then to define additional regions of interest and apply Boolean logic operators to the tract reconstruction. For example, if the reconstructed pathway passes through ROI1 AND ROI2 but not ROI3, then retain it. This approach was first described by Conturo et al. (1999).

Clearly, the success of the tract reconstructions is heavily dependent on the skill and neuroanatomical knowledge of the operator who has to ensure that in placing the ROIs, the only tracts that pass the Boolean logic filtering process belong to the fasciculus of interest. However, despite this operator-dependence, such an approach can undoubtedly produce anatomically faithful reconstructions of white matter fasciculi (e.g., Catani et al., 2002; Mori et al., 2002) and has proven to be useful in a range of applications (see also Catani and Thiebaut de Schotten, 2008, this issue; Epelbaum et al., 2008, this issue; Thiebaut de Schotten et al., 2008, this issue; Doricchi et al., 2008, this issue; Doron and Gazzaniga, 2008, this issue; Catani and Mesulam, 2008, this issue). Fig. 7 shows examples of the types of tract reconstructions that are possible using deterministic tracking (Catani and Ffytche, 2005).

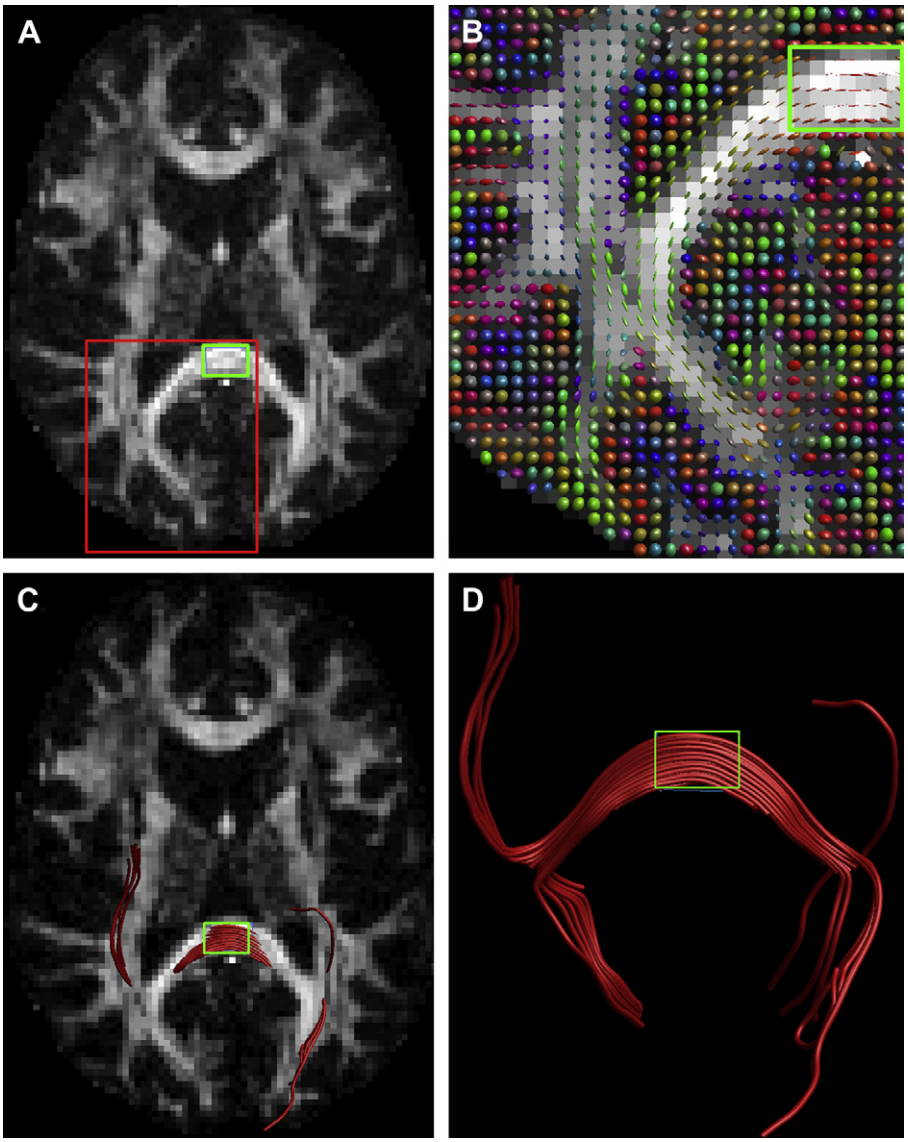

Fig. 6 – Example of deterministic tractography. The user will select a ROI in tissue with high anisotropy (highlighted by the green box in A). In B, the section highlighted in A by the red box has been magnified and the diffusion tensor ellipsoids superimposed (coloured according to the orientation of the principal eigenvector). Just by using the naked eye, one can start to trace pathways through the tensor field. There are clearly pathways projecting posteriorly and others projecting anteriorly. In C, the trajectory reconstructions for the seed voxels are shown. As the tracts pass in and out of the plane of the screen, it is difficult to appreciate the three-dimensional nature of the result, which is shown in isolation in D, revealing indeed two main populations of trajectories – those crossing the splenial midline and projecting anteriorly and those crossing the midline and projecting posteriorly.

Having introduced the concepts of the diffusion tensor model and deterministic tracking, and having extolled their virtues, we now focus on some of the shortcomings and motivate the development of 'probabilistic' tracking algorithms.

9. Limitations of fibre tracking with the deterministic approach

There have been two main criticisms levelled at the deterministic approach. First, deterministic approaches produce only one reconstructed trajectory per seed point, and therefore branching of fasciculi will not, in general, be represented. (Although by placing lots of seedpoints at sub-voxel locations in the 'stem' of the tract before it branches, it could be argued that branching of the fasciculus, as a whole, can be depicted.) Second, there is no indication of the confidence that one can assign to a reconstructed trajectory. This is somewhat of a shortcoming as there is uncertainty associated with each estimate of ε_1 (Basser, 1997; Jones, 2003) and this uncertainty is non-uniform throughout the brain (Jones, 2003).

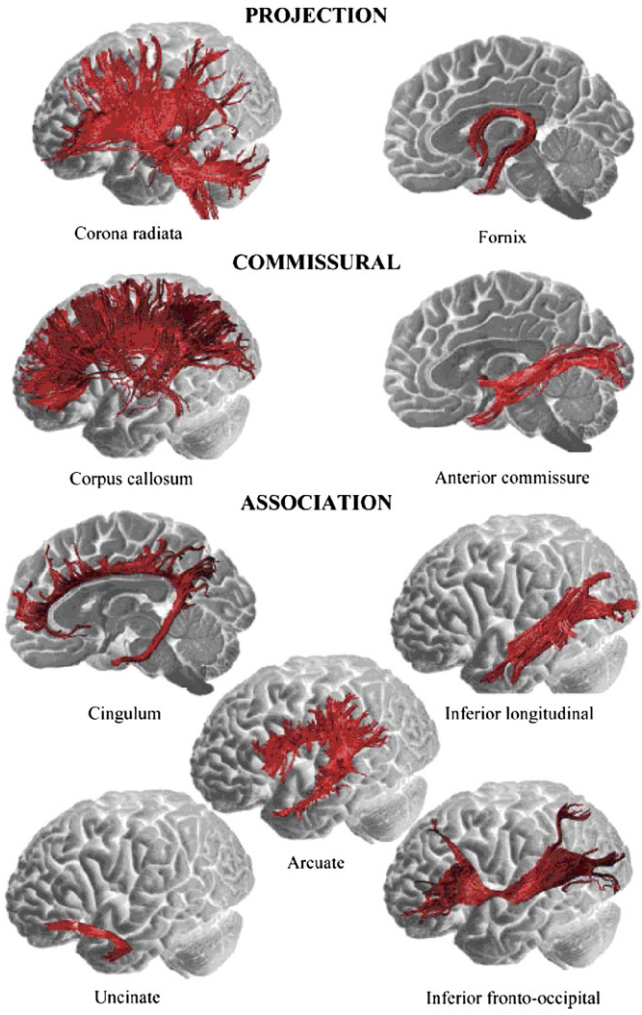

Fig. 7 – Example of tract reconstructions performed using deterministic fibre tracking. Each individual streamline reconstruction is visualized as a three-dimensional tube and lighting added to enhance the three-dimensional visualization and provide a better interpretation of tract topology (image from Catani and Ffytche, 2005).

Fig. 8 shows a reconstruction of the mean (central axis) and 95% confidence intervals (solid cone) in the estimate of the principal eigenvector at each voxel.

In the deep white matter, where there is a single dominant fibre pathway (e.g., the genu of the corpus callosum), the confidence interval is very small and the 'cone of uncertainty' is very tight. Conversely, in CSF-filled regions and in gray matter, the uncertainty in fibre orientation is extremely large. More importantly, even within the white matter, there are regions where the uncertainty in fibre orientation is moderately high. These tend to correspond to regions where the anisotropy of the voxel-averaged tensor is low, which in turn tends to occur where there is more than one dominant fibre orientation within the voxel. Thus, on repeat scanning of the subject, one would obtain a *distribution* of estimates of fibre orientation, with the width of that distribution varying from point to point.

10. Probabilistic tracking approaches

The majority of 'probabilistic' algorithms work in the same way. Instead of reconstructing just a single trajectory from a given seedpoint (as is done in deterministic tractography), they propagate a large number of pathways (either sub-voxel to sub-voxel, or in larger voxel-to-voxel steps) from the seedpoint. At each stage in the stepping process that evolves the path, the direction in which to step next is drawn from a *distribution* of possible orientations. The end result is a set of multiple pathways passing through the seedpoint which is then conventionally summarized by assigning to each voxel the percentage of pathways, launched from the seedpoint, that pass through the voxel.

Criteria for the termination of tracking tend to be slightly different for probabilistic algorithms than for deterministic algorithms. The latter most frequently use a (arbitrary) threshold on anisotropy (e.g., FA $\geq$ 0.15) so as to ensure that the principal eigenvector is relatively well defined and that the uncertainty in the principal eigenvector is not unacceptably high. Additionally, they *may* set a (again arbitrary) threshold on the angle through which the trajectory may turn on successive steps. As probabilistic algorithms are not so dependent on having a well defined principal eigenvector, they typically do not have an anisotropy threshold included in the termination criteria. This facilitates the launching of trajectories from, and reconstruction of trajectories into, areas of low anisotropy such as the gray matter. Typically, therefore, the only stopping criterion is the angular deviation between successive steps (e.g., Behrens et al., 2003; Parker et al., 2003). Without such a threshold, reconstructed trajectories may track back along pathways that have already been visited. Additional stopping criteria may be included, such as the requirement that tracking is terminated if the trajectory enters an area that has already been visited (e.g., Behrens et al., 2003).

The main difference between various probabilistic algorithms is the mechanism by which one draws a sample from the inherent distribution of fibre orientations. Some methods (e.g., Koch et al., 2001; Parker et al., 2003) involve devising an ad hoc relationship between the uncertainty in fibre orientation and the shape of the diffusion tensor. Behrens et al. (2003) derive the distribution in possible estimates of fibre orientation using Bayesian methods, while others (Jones and Pierpaoli, 2005; Lazar and Alexander, 2005) have drawn samples from this distribution by employing bootstrapping methodologies.

The end result is always the same, i.e., a map that essentially attempts to quantify how confident one can be that a pathway can be found, through the data, between each voxel and the seedpoint. In contrast to deterministic approaches, in which the results are presented for a collection of seedpoints within an ROI, probabilistic approaches most typically produce one map per seedpoint. An example of which is presented in Fig. 9.

Of paramount importance is the interpretation of the maps that probabilistic approaches produce. The maps indicate what percentage of pathways, launched from the seedpoint, reach a given voxel. These maps therefore represent the likelihood of a connection through the data, given the samples of the data. The results are therefore strongly dependent on

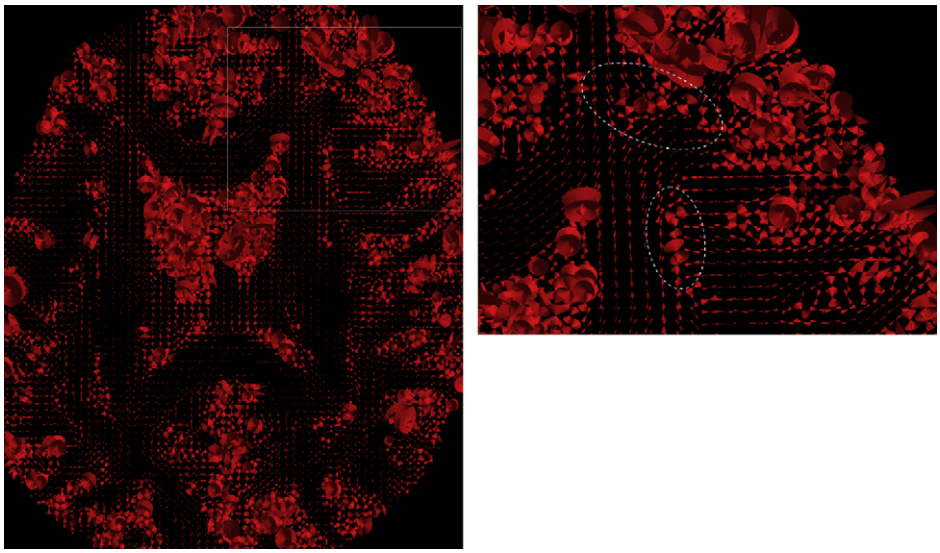

Fig. 8 – Uncertainty in orientation of principal eigenvector. The origin of the magnified region is indicated with the box outlined in dotted lines.

the quality of the data and, if there are shortcomings of the modelling process, or there are systematic errors in the data, then one may obtain highly reproducible (precise), but inaccurate tract reconstructions – which would be represented on a probabilistic tract maps as highly likely. Thus, high likelihood of a connection through the data between a seedpoint and a given voxel on a probabilistic tract map does not necessarily mean that there is a white matter pathway to be found connecting the two points in space. In other words, false positives and false negatives just as problematic in probabilistic tracking as they are in deterministic DT-MRI tracking, as both ultimately use the same streamline algorithm. An example is provided in Fig. 10, which shows results for a seedpoint placed in the cortico-spinal tract. It can be seen that, after passing inferiorly from the seedpoint as far as the pons, the most *likely* path through the data is to continue across the pons and then continue to ascend the contralateral cortico-spinal tract, which is not consistent with known anatomy and therefore inaccurate. One also sees that, by choosing an alternative (more stringent) threshold (Fig. 10C), these

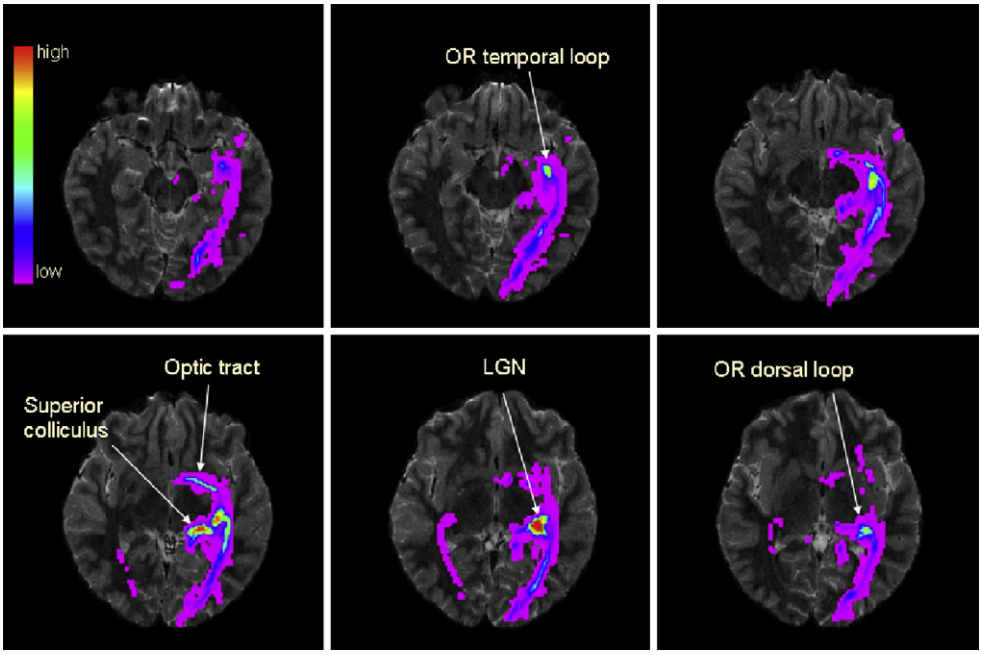

Fig. 9 – Example probabilistic tracking result for a single seedpoint placed in the lateral geniculate nucleus (LGN), revealing high reproducibility of tracking along the optic radiations (ORs), and along the optic tract and superior colliculus (courtesy of Dr Geoff Parker, University of Manchester).

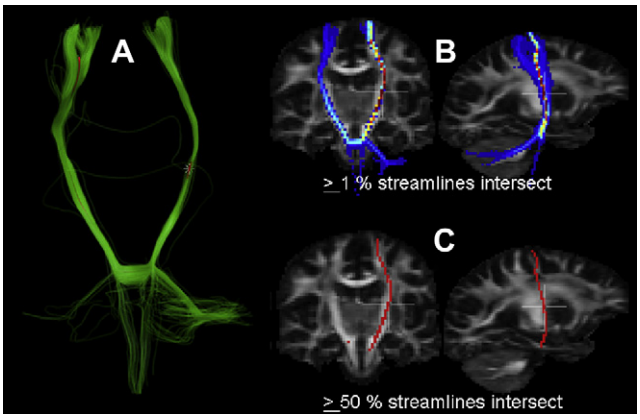

Fig. 10 – Example of reproducible, but artefactual reconstructions. (A) shows the individual streamlines reconstructed as part of the probabilistic algorithm, originated from the single seedpoint indicated by the star. (B) Shows the voxel-intersection maps thresholded at ≥1%. In both (A) and (B), the most visited path after passing inferiorly from the seedpoint is across the pons and up the contralateral cortico-spinal tract. (C) Shows that thresholding at 'high' confidence (≥50% intersection) removes these false positive reconstructions.

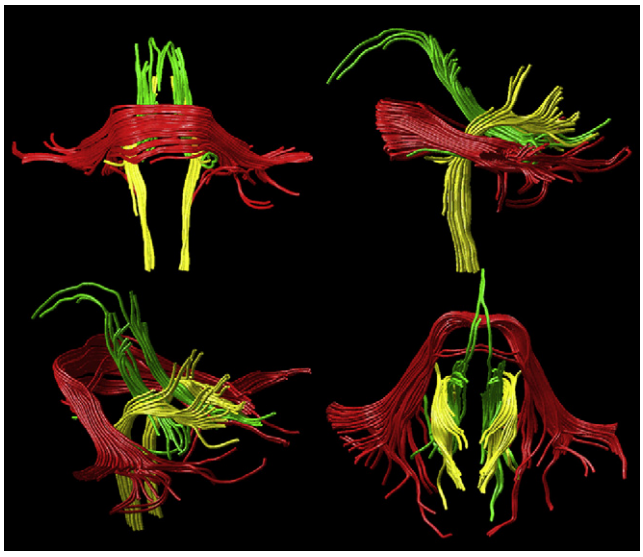

Fig. 11 – Tractography reconstructions with seedpoints placed in inferior (yellow), middle (red) and superior (green) cerebellar peduncles. Although aesthetically pleasing, the anatomy is incorrect. The section of the tract that joins the left and right cerebellar peduncles through the pons (red streamlines) is entirely artefactual (courtesy of Dr Marco Catani, Institute of Psychiatry).

artefactual reconstructions are no longer visualized. However, it is unclear what threshold one should actually employ in these maps.

Obviously, such problems of 'false negatives' are not solely the domain of probabilistic tracking algorithms. As described above, the majority of such algorithms are based on the streamline-following approach employed in deterministic approaches. Thus, it is possible to obtain a highly reproducible topology of (erroneously) reconstructed pathways using multiple seedpoints (the pathway from each individual seedpoint following a similar trajectory to that from its neighbour). This is demonstrated nicely in Fig. 11, in which seedpoints have been placed in the superior, middle and inferior peduncles of the cerebellum. The majority of pathways launched from the middle peduncles cross the midline and form a smooth trajectory connecting the left and right peduncles. This is entirely at odds with known neuroanatomy (Dejerine, 1895; Crosby et al., 1962).

Fig. 10 also shows a problem yet to be resolved in probabilistic tracking – namely, the accumulated error problem. As shown in Fig. 8, there is uncertainty in fibre orientation at each stage in the propagation of the tract. Thus, the error in fibre position will accumulate, and the longer the tract – the greater the accumulated error. Thus, even in a relatively organized and straight fibre pathway such as that presented in Fig. 10, the voxels closest to the seedpoint will always have a higher percentage of reconstructed pathways intersecting them, than those which are further away. If the maps are interpreted simply as showing the likelihood that a path, launched from the seedpoint, will reach a given voxel – then there is absolutely no problem. However, such maps have also been interpreted by many as showing 'anatomical connectivity', and those voxels that have a higher value in the map are considered to be 'more strongly connected' or have 'higher anatomical connectivity'. Consideration of the combined problems of accumulated error and the accuracy *versus* precision issue is sufficient to lead to the conclusion that such interpretations of these maps should be treated with extreme caution. Solutions to the accumulated error problem have been mooted (Morris et al., 2006), but robust approaches that adequately and robustly handle the problem have, to the best of this author's knowledge, remained elusive.

11. Crossing fibres

In terms of systematic errors in the modelling process, a major contributor to this is the inadequacy of the tensor model to characterize fibre orientation when there is more than one fibre population with a voxel. As will be recalled from Fig. 3, the Gaussian tensor model assumes a unimodal displacement probability distribution, where the principal eigenvector is co-aligned with the dominant fibre orientation within a voxel. In regions containing more than one fibre orientation population, a single fibre orientation is inadequate to *completely* characterize the fibre orientations. Thus, alternatives to the tensor model that allow for more than one dominant fibre orientation to be modelled must be used. Solutions can be broadly broken down into approaches: (1) model based approaches, including fitting more than one tensor to the data (Tuch, 2002), deconvolving the idealised response from a single fibre population to extract the distribution of fibre orientations (e.g., Tournier et al., 2004), and attempting to model the intra- and extra-axonal compartments separately (Assaf and Basser, 2005) and (2) model-free approaches, in which the

three-dimensional displacement probability profile is obtained from the data directly (e.g., Wedeen et al., 2005; Tuch, 2004). For a detailed review and comparison of these methods, see Alexander (2005). Fig. 12 shows the efficacy of one of the model-based approaches, spherical harmonic decomposition (Tournier et al., 2004; Tournier et al., 2007) in which the 'fibre orientation density' is extracted and represented in each voxel as surface-rendered shapes that peak along the dominant fibre orientations (in this case, there are up to three major peaks in each voxel). Performing fibre tractography with a tensor model in a medial–lateral direction in the callosal fibres selected here, for example, is doomed to failure as the principal eigenvector orientation is dominated by the contribution from the superior longitudinal fasciculus (SLF).

It is, of course, essential not to just blindly fit a complex model to the data if the data do not support it, and therefore model parsimony measures are required to determine where the more complex models (i.e., multiple fibre orientations) are justified. There are several approaches available for model based approaches, including *F*-test approaches (Parker and Alexander, 2003) and Bayesian automated relevance detection (Behrens et al., 2007). However, without a model (such as in Q-ball imaging (Tuch, 2004)) or diffusion-spectrum imaging (Wedeen et al., 2005), extreme care must be taken to ensure that noise/artefacts in the data do not lead to spikes in the displacement profile that are mistakenly interpreted as representing a fibre bundle to be followed. We should also point out that the inadequacy of the tensor model to fully capture the orientational information is not just limited to having two discrete fibre bundles oriented at a given angle to each other. Rather, the term 'crossing fibres' has become a loosely used term to represent a whole range of fibre architectural paradigms within a voxel including, but not limited to, fibres crossing, 'kissing', splaying – and even single fibre bundles that bend, curve or twist within a voxel.

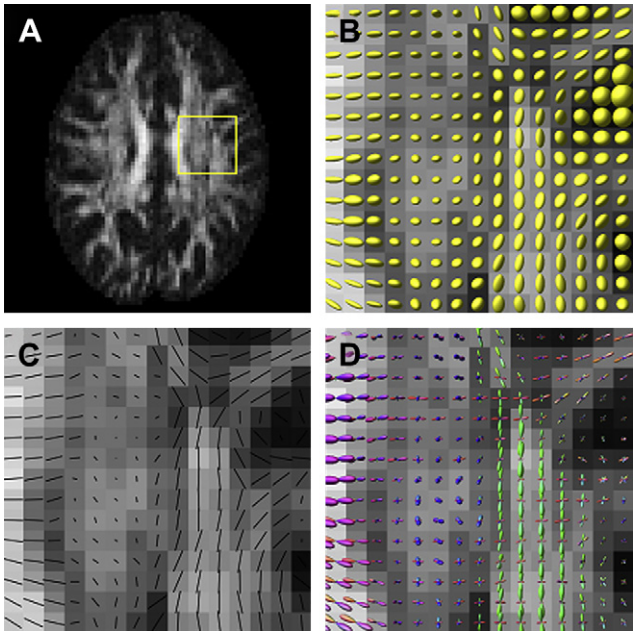

Fig. 12 – Comparison of fibre orientational information extracted from the tensor model and spherical harmonic deconvolution. (A) ROI placed on anisotropy map in a region containing callosal fibres, fibres of corona radiata and fibres of the SLF). (B) The estimated diffusion tensors in each voxel represented as surface-rendered ellipsoids. (C) The 2D-projection of the principal eigenvectors of the diffusion ellipsoids. (D) Estimated fibre orientation density in each voxel, represented as a surface-rendered plot. The three main fibre tracts can be identified: left–right projections from the corpus callosum (in red), anterior–posterior projection of the SLF (green) and inferior–superior projections of the corona radiata (blue). Images courtesy of Donald Tournier, Brain Research Institute, Melbourne, Australia.

How prevalent are such architectural paradigms, and when is the tensor model strictly inadequate? Obviously, the answer to this question depends on the quality of the data as well as the complexity of the tissue, but one can get an approximate idea by employing the aforementioned parsimony measure/model selection strategies. By using a Bayesian modelling approach to extend their previous model, Behrens et al. (2003, 2007) estimate that over one third of voxels in the brain exhibit marked departures from the Gaussian diffusion behaviour characterized by the tensor model. Fig. 13 shows the prevalence in an axial slice at the level of the body of the corpus callosum.

Despite a considerable increase in global research activity over the last 5 years in developing algorithms to resolve these crossing fibre paradigms (at least to the extent that they are better characterized than by the single-tensor model), the number of tractography studies that have actually utilized such information is surprisingly limited (Parker and Alexander, 2003, 2005; Hosey et al., 2005; Schmahmann et al., 2007; Behrens et al., 2007). This could be partly explained by the difficulty in knowing how to handle the new information that is provided. The results from many 'fibre crossing' analysis techniques are often not sharply defined fibre orientations, but rather continua of fibre orientations with multiple modes. Nevertheless, a small handful of groups have explored fibre tracking with crossing fibre information. Fig. 14 shows the results of Parker and Alexander's (2005) attempts to reconstructing the projections of the left motor strip combining a Monte Carlo probabilistic tracking algorithm (Parker et al., 2003) with persisent angular structure MRI (PAS-MRI) (Jansons and Alexander, 2003) – a technique that aims to resolve multiple fibre populations within a voxel. This is presented in Fig. 14, along with a representation (taken from Catani, 2007) of one of the 'classic' reconstruction problems with single-tensor deterministic tracking algorithms, namely the failure of the method to reconstruct lateral aspects of the projection system. It is important to point out that in Fig. 13A, the seedpoints for tractography were placed deep within white matter, where the anisotropy is high and the uncertainty in fibre orientation is low (as is the norm when using deterministic tracking algorithms), which is in stark contrast to the case in Fig. 13B, in which tracts are launched from an area of low anisotropy (the cortex) where uncertainty in fibre orientation is high. It is important to re-iterate that most 'probabilistic' algorithms are based on the same streamlining algorithms used in deterministic approaches (the basic streamlining algorithm was the same for the results presented in Fig. 14). Thus, if one had launched a large number of

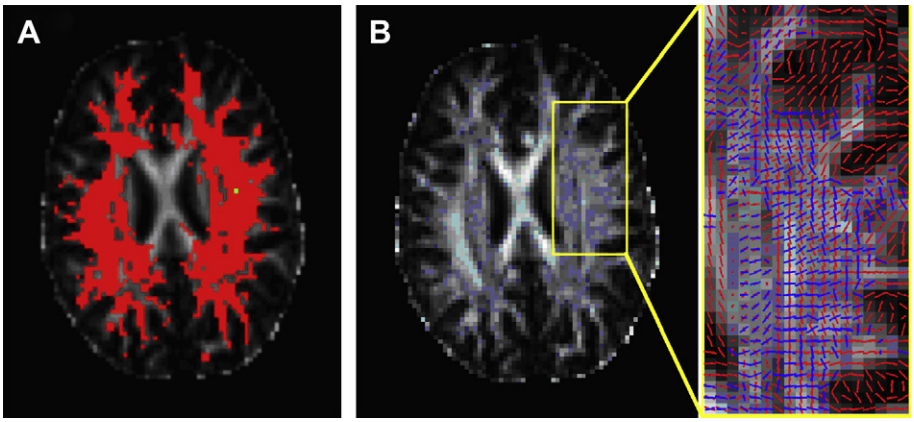

Fig. 13 – Demonstration of the ubiquity of the 'crossing fibre' problem. (A) Voxels where more the modelling of more than one fibre orientation is supported by the data are highlighted in red. (B) Close up of crossing fibre bundles with dominant orientations in red and blue.

densely seeded tracts from the cortex using the deterministic algorithm in Fig. 14A, with a lower anisotropy threshold for initiation and termination of tracking, a similar pattern of 'spread' would be obtained in the resultant tract distribution as shown in Fig. 14B. In other words, in regions of low anisotropy, one will expect 'spread' of tracts simply by virtue of the high uncertainty in fibre orientation (see Fig. 8). Although incorporation of crossing fibre information undoubtedly aids in more accurate tract reconstructions, it clearly does not provide a complete solution. For example, while in the side ipsilateral to the ROI the fibres leaving the motor strip are well represented, on the other side the corpus callosum fails to reach the entire motor strip where, according to classical neuroanatomy and electrophysiology, one expects callosal fibre projections. In addition to such false negatives, there are also false positives, i.e., the result includes white matter that is either not part of the motor system or is unlikely to have real connections with the selected seed region.

As a final demonstration of the importance of building crossing fibre information into fibre tracking algorithms for certain pathways, Fig. 15 shows the results obtained by Behrens et al. (2007) in attempting to reconstruct fibre pathways between medial geniculate nucleus of thalamus and primary auditory cortex using the tracking algorithm described in Behrens et al. (2003) with and without crossing fibre information. The result is striking in that, while it was not possible to reconstruct any pathways in any of the nine subjects without crossing fibre information, at least some fibres could be reconstructed between the two regions of interest in all subjects when crossing fibres information are included.

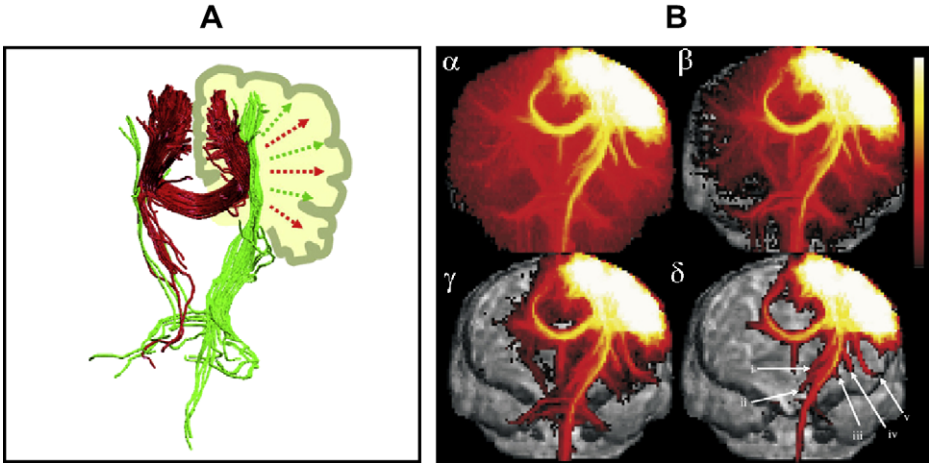

Fig. 14 – (A) The classic appearance of deterministic streamline tracking results failing to reconstruct the lateral aspects of the cortico-spinal projections (green arrows and green tracts) and corpus callosum (red arrows and red tracts) (modified from Catani, 2007). (B) A result obtained by employing crossing fibre information into a probabilistic tracking algorithm (taken from Parker and Alexander, 2005 with permission). Coronal projections of left motor strip connectivity are shown at different thresholds. Logarithmic colour scale: (α) $0.0 < p < 1.0$, (β) $0.027 < p < 1.0$, (γ) $0.074 < p < 1.0$, and (δ) $0.20 < p < 1.0$. Major apparent connections identified include (i) thalamus, (ii) subthalamic nucleus, (iii) globus pallidus, (iv) putamen and (v) Wernicke's area.

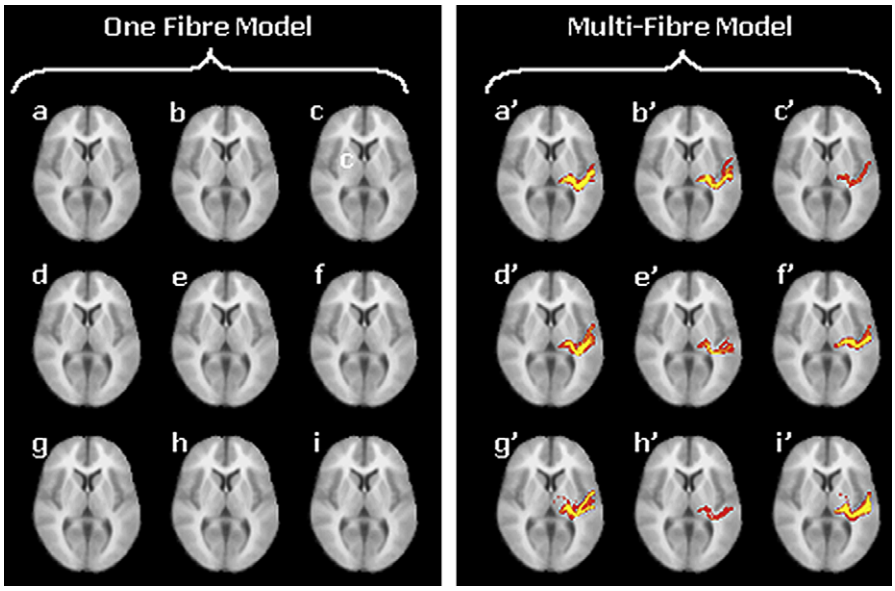

Fig. 15 – Tracking of the acoustic radiations in nine individuals (a–i) between medial geniculate nucleus of thalamus and primary auditory cortex with single fibre model (left panel) and multi-fibre (right panel) tractography. An axial maximum intensity projection is shown. Voxels are colour coded from 10 (red) to 50 (yellow) samples passing through the voxel. The single fibre tractography was not able to find any connections that reached the target in any of the nine subjects, but the multi-fibre model was able to find connections in all of the same nine subjects.

12. Conclusion

In this final section, we would like to summarize the successes and strengths of diffusion-based imaging techniques for studying white matter connections, as well as the weaknesses and consider some of the most pressing problems that must be addressed before we can reliably study the *entire* brain in a hodological, but non-invasive, manner.

At present, diffusion-based MR imaging techniques are the only non-invasive techniques that show promise for studying the pathways and connections of human brain. It has been shown by many groups that within the major white matter pathways, it is possible to gain three-dimensional reconstructions of fasciculi that are remarkably close to those obtained by post-mortem dissection. However, with basic deterministic tracking and the tensor model, it is impossible to accurately reconstruct all the major pathways, especially where fibres branch and cross. The various methods being developed for resolving fibre crossing information are intriguing in that they partly ameliorate the limitations of the tensor model. However, there is still a lot of work to be done. Currently, it is impossible to differentiate between, for example two fibres that cross in a voxel from two fibres that 'kiss' within the voxel. Similarly, a single fibre bundle that changes its direction with the voxel (e.g., a simple bend) introduces multiple 'fibre orientations' which will be reconstructed by most methods as a symmetrical multi-peaked displacement probability profile, or fibre orientation density function, with some of the peaks pointing to pathways in which the fibres do not actually go. Further, it is not always clear which peak one should follow when propagating a path through these complex architectures and so the usual approach is to adopt some intuitive, albeit *ad hoc*, rule about choosing the peak that subtends the smallest angle. So, although these emerging methods are an improvement on the information provided by the tensor model, they are by no means a complete solution and a lot more work is needed before they can unequivocally resolve the ubiquitous topological ambiguities that are present in the white matter of the human brain.

This article has also discussed the concept of probabilistic tractography, but has intentionally steered clear of making ambitious statements about the potential applications. No one can argue against the fact that these methods inform the user as to how likely it is that a given pathway be found *through the data set*. However, the hopes and needs of neuroscientists taking a hodological approach stretch beyond this information. They want to be able to assess the *integrity* of white matter networks, and to quantify the *strength* of connection. This perhaps explains the prevalence of the term 'connectivity' used in association with fibre tractography studies, with areas with high voxel scores on probabilistic tract maps being described as having 'high anatomical connectivity' to the seedpoint. While incorporating crossing fibre information undoubtedly helps in reducing false negatives, the same cannot always be said of false positives (see the discussion in Behrens et al., 2007 for some rounded comments on this issue). Thus, we must not confuse accuracy with precision. For a robust assessment of white matter pathways, we need to have a high degree of both. Even if the two measures went hand in hand (which, as shown in Figs. 10 and 11, is not always the case), we then have to interpret how does the 'score' in a probabilistic tract map

correlate with the aspect of 'connectivity' that we are attempting to quantify and what are the functional consequences of changes in that score.

One of the biggest problems that remains to be addressed is the distance normalization problem. Consider the portion of the cortico-spinal tract that runs either side of the seedpoint in Fig. 10 from the cortex to *just before* the pons. In this section, there is only one white matter pathway, pathways cannot branch off to join other networks. Thus, any information that is being carried along the pathway should be carried along the entire length of this section (i.e., information doesn't get 'lost' along the way), thus the 'functional connectivity' provided by this pathway is uniform along the section under consideration. However, the probabilistic map suggests that the 'anatomical connectivity' (if this is how we choose to interpret the map) drops off either side of the seedpoint. The biological/functional consequences of such a phenomenon are hard to fathom. On a related note, while probabilistic algorithms can reveal branching patterns that deterministic approaches cannot, one again has to be careful about interpretation of voxel scores 'downstream' of a branch, e.g., if 1000 tracts reach a branching point, and 50% pass down one branch and 50% down the other, the resulting 'connectivity' can be no greater than 50% of what it was prior to the branch. These problems are familiar to the diffusion community, but solutions are yet to be found.

Surprisingly, given the amount of effort invested in developing and refining tracking algorithms, very little has been done to attempt to compare those tract reconstructions obtained with non-invasive diffusion methods, with those obtained by classical neuroanatomical dissection. One notable exception is that of Lawes et al. (2007a) and Lawes et al. (2007b, in press). Although painstaking, direct comparisons between 'virtual in vivo dissection' and classical neuroanatomical dissections such as reported by Lawes are essential to gain a better understanding on accuracy and false negatives/false positives. The reader is referred to this work for clear examples substantiating the claim that in the major white matter fasciculi, one can obtain reconstructions that are anatomically very plausible.

In conclusion, the assessment of white matter pathways using diffusion-based imaging methods has come a long way since the initial observation of diffusion anisotropy 17 years ago (Moseley et al., 1990b). However, tractography does not provide a direct measure of connectivity in the human brain although in certain circumstances it may provide information that is related to underlying cerebral connectivity. Clearly, there is still a fair way to go before we can reliably compete with the dissectionists of yesteryear in assessing the connections of the human brain.

REFERENCES

Aldroubi A and Basser PJ. Reconstruction of vector and tensor fields from sampled discrete data. *Contemporary Mathematics*, 247: 1–15, 1999.

Alexander DC. Multiple-fiber reconstruction algorithms for diffusion MRI. *Annals of New York Academy of Sciences*, 1064: 113–133, 2005.

Assaf Y and Basser PJ. Composite hindered and restricted model of diffusion (CHARMED) MR imaging of the human brain. *NeuroImage*, 27: 48–58, 2005.

Basser PJ, Mattiello J, and Le Bihan D. Estimation of the effective self-diffusion tensor from the NMR spin echo. *Journal of Magnetic Resonance Series B*, 103: 247–254, 1994.

Basser PJ. Quantifying errors in fiber tract direction and diffusion tensor field maps resulting from MR noise. In: *Proceedings of the Fifth Annual Meeting of ISMRM*, Vancouver, Canada; 1997. p. 1740.

Basser PJ, Pajevic S, Pierpaoli C, Duda J, and Aldroubi A. In vivo tractography using DT-MRI data. *Magnetic Resonance in Medicine*, 44: 625–632, 2000.

Basser PJ and Pierpaoli C. Microstructural and physiological features of tissue elucidated by quantitative-diffusion-tensor MRI. *Journal of Magnetic Resonance B*, 111: 209–219, 1996.

Beaulieu C. The basis of anisotropic water diffusion in the nervous system – a technical review. *NMR in Biomedicine*, 15: 435–455, 2002.

Beaulieu C and Allen PS. Determinants of anisotropic water diffusion in nerves. *Magnetic Resonance in Medicine*, 31: 394–400, 1994a.

Beaulieu C and Allen PS. Water diffusion in the giant axon of the squid: implications for diffusion-weighted MRI of the nervous system. *Magnetic Resonance in Medicine*, 32: 579–583, 1994b.

Beaulieu C and Allen PS. An in vitro evaluation of the effects of local magnetic-susceptibility-induced gradients on anisotropic diffusion in nerve. *Magnetic Resonance in Medicine*, 36: 39–44, 1996.

Behrens TE, Johansen-Berg H, Woolrich MW, Smith SM, Wheeler-Kingshott CA, Boulby PA, Barker GJ, Sillery EL, Sheehan K, Ciccarelli O, Thompson AJ, Brady JM, and Matthews PM. Non-invasive mapping of connections between human thalamus and cortex using diffusion imaging. *Nature Neuroscience*, 6: 750–757, 2003.

Behrens TEJ, Johansen-Berg H, Jbabdi S, Rushworth MFS, and Woolrich MW. Probabilistic diffusion tractography with multiple fibre orientations: what can we gain? *NeuroImage*, 34: 144–155, 2007.

Brown R. A brief account of microscopical observations made in the months of June, July and August 1827 on the particles contained in the pollen of plants; and on the general existence of active molecules in organic and inorganic bodies. *Philosophical Magazine*, 4: 161, 1828.

Catani M and Thiebaut de Schotten M. A diffusion tensor tractography atlas for virtual in vivo disconnections. *Cortex*, 44: 1105–1132, 2008.

Catani M and Mesulam M. The arcuate fasciculus and the disconnection theme in language and aphasia: history and current state. *Cortex*, 44: 953–961, 2008.

Catani M, Howard R, Pajevic S, and Jones DK. Virtual in vivo interactive dissection of white matter fasciculi in the human brain. *NeuroImage*, 17: 77–94, 2002.

Catani M and ffytche D. The rises and falls of disconnection syndromes. *Brain*, 128: 2224–2239, 2005.

Catani M. From hodology to function. *Brain*, 130: 602–605, 2007.

Chenevert TL, Brunberg JA, and Pipe JG. Anisotropic diffusion within human white matter: demonstration with NMR techniques in vivo. *Radiology*, 177: 401–405, 1990.

Cleveland GG, Chang DC, Hazelwood CF, and Rorschach HE. Nuclear magnetic resonance measurement of skeletal muscle. Anisotropy of the diffusion coefficient of the intracellular water. *Biophysical Journal*, 16: 1043–1053, 1976.

Conturo TE, Lori NF, Cull TS, Akbudak E, Snyder AZ, Shimony JS, Mckinstry RC, Burton M, and Raichle ME. Tracking neuronal fiber pathways in the living human brain. *Proceedings of the*

National Academy of Sciences United States of America, 96: 10422–10427, 1999.
Crosby EC, Humphrey T, and Lauer EW. *Correlative Anatomy of the Nervous System*. New York: The Macmillian Company, 1962.
Dejerine J. *Anatomie des centres nerveux vol. 1*. Paris: Rueff et Cie, 1895.
Doran M, Hajnal J, Van Bruggen N, King MD, Young IR, and Bydder GM. Normal and abnormal white matter tracts shown by MR imaging using directional diffusion weighted sequences. *Journal of Computer Assisted Tomography*, 14: 865–873, 1990.
Douek P, Turner R, Pekar J, Patronas NJ, and Le Bihan D. MR colour mapping of myelin fiber orientation. *Journal of Computer Assisted Tomography*, 15: 923–929, 1991.
Doricchi F, Thiebaut de Schotten M, Tomaiuolo F, and Bartolomeo P. White matter (dis)connections and gray matter (dys)functions in visual neglect: Gaining insights into the brain networks of spatial awareness. *Cortex*, 44: 983–995, 2008.
Doron KW and Gazzaniga MS. Neuroimaging techniques offer new perspectives on callosal transfer and interhemispheric communication. *Cortex*, 44: 1023–1029, 2008.
Epelbaum S, Pinel P, Gaillard R, Delmaire C, Perrin M, Dupont S, Dehaene S, and Cohen L. Pure alexia as a disconnection syndrome: New diffusion imaging evidence for an old concept. *Cortex*, 44: 962–974, 2008.
Einstein A. Über die von der molekularkinetischen Theorie der Wärme gefordete Bewegung von in ruhenden Flüssigkeiten suspendierten Teilchen. *Ann Physik*, 4: 549–590, 1905.
Gulani V, Webb AG, Duncan ID, and Lauterbur PC. Apparent diffusion tensor measurements in myelin-deficient rat spinal cords. *Magnetic Resonance in Medicine*, 45: 191–195, 2001.
Hansen JR. Pulsed NMR study of water mobility in muscle and brain tissue. *Biochimica et Biophysica Acta*, 230: 482–486, 1971.
Hong X and Dixon WT. Measuring diffusion in inhomogeneous systems in imaging mode using antisymmetric sensitizing gradients. *Journal of Magnetic Resonance*, 99: 561–570, 1992.
Hosey T, Williams G, and Ansorge R. Inference of multiple fiber orientations in high angular resolution diffusion imaging. *Magnetic Resonance in Medicine*, 54: 1480–1489, 2005.
Jansons KM and Alexander DC. Persistent angular structure: new insights from diffusion MRI data. *Information Processing in Medical Imaging*, 18: 672–683, 2003.
Jones DK, Williams S, and Horsfield MA. Full representation of white-matter fibre direction on one map via diffusion tensor analysis. In: *Book of Abstracts: Fifth Annual Meeting of the International Society of Magnetic Resonance in Medicine*. Berkeley, CA: ISMRM, 1997: 1741.
Jones DK, Simmons A, Williams SCR, and Horsfield MA. Non-invasive assessment of axonal fiber connectivity in the human brain via diffusion tensor MRI. *Magnetic Resonance in Medicine*, 42: 37–41, 1999.
Jones DK. Determining and visualizing uncertainty in estimates of fiber orientation from diffusion tensor MRI. *Magnetic Resonance in Medicine*, 49: 7–12, 2003.
Jones DK and Pierpaoli C. Confidence mapping in deterministic DT-MRI tractography. *Magnetic Resonance in Medicine*, 53: 1143–1149, 2005.
Koch M, Glauche V, Finsterbusch J, Nolte U, Frahm J, and Buchel C. Estimation of anatomical connectivity from diffusion tensor data. *NeuroImage*, 13: S176, 2001.
Lawes IN, Barrick TR, Murugam V, and Clark CA. Atlas based segmentation of white matter tracts of the human brain using diffusion tensor tractography and comparison with classical dissection. In International Society of Magnetic Resonance in Medicine 15th Annual Meeting, Abstract #229, Berlin, Germany, 2007a.
Lawes IN, Barrick TR, Murugam V, Spierings N, Evans D, Song M, and Clark CA. Atlas based segmentation of white matter tracts of the human brain using diffusion tensor tractography and comparison with classical dissection. *NeuroImage*, 2007b, in press.
Lazar M and Alexander AL. Bootstrap white matter tractography (BOOT-TRAC). *NeuroImage*, 15: 524–532, 2005.
Le Bihan D and Breton E. Imagerie de diffusion in vivo par résonance magnétique nucléaire. *Compte Rendus de l'Académie de Sciences Paris*, 301: 1109–1112, 1985.
Lian J, Williams DS, and Lowe IJ. Magnetic resonance imaging in the presence of background gradients and imaging of background gradients. *Journal of Magnetic Resonance Series A*, 106: 65–74, 1994.
Ludwig E and Klingler J. *Atlas Cerebri Humani*. Basel: S. Karger, 1956.
Makris N, Worth AJ, Sorenson AG, Papadimitriou GM, Wu O, Reese TG, Wedeen VJ, Davis TL, Stakes JW, Caviness VS, Kaplan E, Rosen BR, Pandya DN, and Kennedy DN. Morphometry of in vivo human white matter association pathways with diffusion weighted magnetic resonance imaging. *Annals of Neurology*, 42: 951–962, 1997.
Mori S, Crain BJ, Chacko VP, and Van Zijl PC. Three dimensional tracking of axonal projections in the brain by magnetic resonance imaging. *Annals of Neurology*, 45: 265–269, 1999.
Mori S, Kaufmann WE, Davatzikos C, Stieltjes B, Amodei L, Fredericksen K, Pearlson GD, Melhem ER, Solaiyappan M, Raymond GV, Moser HW, and Van Zijl PC. Imaging cortical association tracts in the human brain using diffusion-tensor-based axonal tracking. *Magnetic Resonance in Medicine.*, 47: 215–223, 2002.
Morris DM, Embleton KV, and Parker GJ. Definition of connection significance using probabilistic tractography. In *Proceedings of the 14th Annual Meeting of ISMRM,* Seattle, USA, 2006: 434.
Moseley ME, Cohen Y, Mintorovitch J, Chileuitt L, Shimizu H, Kucharczyk J, Wendland MF, and Weinstein PR. Early detection of regional brain ischemia in cats: comparison of diffusion- and T2-weighted MRI and spectroscopy. *Magnetic Resonance in Medicine*, 14: 330–346, 1990a.
Moseley ME, Cohen Y, and Kucharczyk J. Diffusion weighted MR imaging of anisotropic water diffusion in cat central nervous system. *Radiology*, 187: 439–446, 1990b.
Nakada T, Matsuwaza H, and Kwee IL. Magnetic resonance axonography of the rat spinal-cord. *NeuroReport*, 5: 2053–2056, 1994.
Pajevic S and Pierpaoli C. Colour schemes to represent the orientation of anisotropic tissues from diffusion tensor data: application to white matter fiber tract mapping in the human brain. *Magnetic Resonance in Medicine*, 43: 526–540 (Erratum appears in *Magnetic Resonance in Medicine* 43: 921–921, 1999), 1999.
Pajevic S, Basser PJ, and Aldroubi A. A continuous tensor field approximation for DT-MRI data. In: *Book of Abstracts: Seventh Annual Meeting of the International Society for Magnetic Resonance in Medicine*. Berkeley, CA: ISMRM, 2001: 1535.
Parker GJM. Tracing fiber tracts using fast marching. In: *Book of Abstracts: Eighth Annual Meeting of the International Society for Magnetic Resonance in Medicine*. Berkeley, CA: ISMRM, 2000: 85.
Parker GJ, Haroon HA, and Wheeler-Kingshott CA. A framework for a streamline-based probabilistic index of connectivity (PICO) using a structural interpretation of MRI diffusion measurements. *Journal of Magnetic Resonance Imaging*, 18: 242–254, 2003.
Parker GJM and Alexander DC. Probabilistic Monte Carlo based mapping of cerebral connections utilising whole-brain crossing fibre information. *Information Processing in Medical Imaging*, 18: 684–695, 2003.

Parker GJM and Alexander DC. Probabilistic anatomical connectivity derived from the microscopic persistent angular structure of cerebral tissue. *Philosophical Transactions of the Royal Society London, Series B: Biological Sciences*, 360: 893–902, 2005.

Pierpaoli C. Oh no! One more method for colour mapping of fiber tract direction using diffusion MR imaging data. In: *Book of Abstracts: Fifth Annual Meeting of the International Society of Magnetic Resonance in Medicine*. Berkeley, CA: ISMRM, 1997: 1743.

Poupon C, Clark CA, Frouin V, Regis J, Bloch I, Le Bihan D, and Mangin J. Regularization of diffusion-based direction maps for the tracking of brain white matter fasciculi. *NeuroImage*, 12: 184–195, 2000.

Prayer D, Roberts T, Barkovich AJ, Prayer L, Kucharczyk J, Moseley M, and Arieff A. Diffusion-weighted MRI of myelination in the rat brain following treatment with gonadal hormones. *Neuroradiology*, 39: 320–325, 1997.

Schmahmann JD, Pandya DN, Wang R, Dai G, D'arceuil HE, de Crespigny AJ, and Wedeen VJ. Association fibre pathways of the brain: parallel observations from diffusion spectrum imaging and autoradiography. *Brain*, 130: 630–653, 2007.

Stejskal EO and Tanner JE. Spin diffusion measurements: spin echoes in the presence of a time-dependent field gradient. *Journal of Chemical Physics*, 42: 288–292, 1965.

Thomsen C, Henriksen O, and Ring P. *In vivo* measurement of water self diffusion in the human brain by magnetic resonance imaging. *Acta Radiologica*, 28: 353–361, 1987.

Thiebaut de Schotten M, Kinkingnéhun S, Delmaire C, Lehéricy S, Duffau H, Thivard L, et al. Visualization of disconnection syndromes in humans. *Cortex*, 44: 1097–1103, 2008.

Tournier J-D, Calamante F, Gadian DG, and Connelly A. Direct estimation of the fiber orientation density function from diffusion-weighted MRI data using spherical deconvolution. *NeuroImage*, 23: 1176–1185, 2004.

Tournier JD, Calamante F, and Connelly A. Robust determination of the fibre orientation distribution in diffusion MRI: non-negativity constrained super-resolved spherical deconvolution. *NeuroImage*, 35: 1459–1472, 2007.

Tuch DS, Belliveau JW, and Wedeen VJ. A path integral approach to white matter tractography. In: *Book of Abstracts: Eighth Annual Meeting of the International Society for Magnetic Resonance in Medicine*. Berkeley, CA: ISMRM, 2000: 791.

Tuch DS, Reese TG, Wiegell MR, Makris N, Belliveau JW, and Wedeen VJ. High angular resolution diffusion imaging reveals intravoxel white matter fiber heterogeneity. *Magnetic Resonance in Medicine*, 48: 577–582, 2002.

Tuch DS. Q-ball imaging. *Magnetic Resonance in Medicine*, 52: 1358–1372, 2004.

Wedeen VJ, Hagmann P, Tseng W-YI, Reese TG, and Weisskoff RM. Mapping complex tissue architecture with diffusion spectrum magnetic resonance imaging. *Magnetic Resonance in Medicine*, 54: 1377–1386, 2005.

Wimberger DM, Roberts TP, Barkovich AJ, Prayer LM, Moseley ME, and Kucharczyk J. Identification of "premyelination" by diffusion-weighted MRI. *Journal of Computer Assisted Tomography*, 19: 28–33, 1995.